Computational Mechanics 17 (1996) 326–334 © Springer-Verlag 1996

Development of shear bands during the perforation of a steel plate

R. C. Batra, Z. Peng

Abstract We have analysed the development of shear bands during the perforation of a steel plate by a massive rigid punch. The contact surfaces are modeled as smooth and the steel is modeled as a thermoviscoplastic material that hardens with an increase in the plastic strain and plastic strain-rate but softens due to the rise in its temperature. The effect of punch speed, the clearance between the punch and the back supports, and the radius of the periphery of the punch nose on the development of bands is delineated.

1 Introduction

Even though Tresca (1878) reported the development of shear bands during the hot forging of platinum more than a century ago, the activity in this field picked up since the time Zener and Hollomon (1944) observed 32 μm wide shear bands during the punching of a hole in a low carbon steel plate. Zener and Hollomon also pointed out that during the punching process, heat produced because of the intense plastic deformations of the material soften it and once this softening equals the hardening of the material due to strain and strain-rate effects, it becomes unstable. The study of shear bands is important because once these bands have developed, subsequent deformations of the body are concentrated in these narrow regions and the strength of the rest of the body is not fully utilized. Also, shear bands precede shear fractures and are the primary mode of failure in ductile materials under dynamic loading. Subsequently Moss (1981) conducted tests similar to those of Zener and Hollomon (1944) and reported that strain-rates of the order of 10^5/sec occur within the shear band. Chou et al. (1991) have performed controlled penetration tests and have measured the length of the band ahead of the punch surface.

Duffy and co-workers (1984, 1988) have measured the time-history of the temperature rise and the plastic strain during the development of a shear band in a thin-wall steel tube that is dynamically twisted. Other types of test specimens and loading conditions have been employed by Kalthoff (1987) and Mason et al. (1994).

Several investigators have analysed the initiation and growth of shear bands analytically and numerically; we refer the reader to the proceedings of three symposia edited by Zbib et al. (1992), Armstrong et al. (1994) and Batra and Zbib (1994) and a book by Bai and Dodd (1992) for a list of references on the subject. Here we use an adaptive mesh refinement technique to analyse the formation of shear bands during the perforation of a steel plate. It is found that the radius of the periphery of the nose of the punch has a noticeable effect upon the length of the band ahead of the punch surface. Also the clearance between the punch and the back supports affects significantly when a band initiates, and it determines the profile of the mantle of the plug ejected out of the plate. We note that there is no a priori defect introduced to initiate a shear band.

2 Formulation of the problem

We use a cylindrical coordinate system to analyse axisymmetric deformations of a steel plate impacted at normal incidence by a massive rigid cylindrical rod and assume that the contact surfaces are smooth; a schematic sketch of the problem studied is shown in Fig. 1 wherein dimensions of different parts are also given. We use an updated Lagrangian description of motion. Equations governing thermomechanical deformations of the steel plate are

$$(\rho J)^{\cdot} = 0, \tag{1}$$

$$\rho_0 \dot{\mathbf{v}} = \mathrm{Div}\,\mathbf{T}, \tag{2}$$

$$\rho_0 \dot{e} = -\mathrm{Div}\,\mathbf{Q} + tr(\mathbf{T}\dot{\mathbf{F}}^T). \tag{3}$$

Equations (1), (2) and (3) express, respectively, the balance of mass, balance of linear momentum and the balance of internal energy. In them ρ is the present mass density of a material particle whose mass density in the reference configuration is ρ_0, $J = \det \mathbf{F}$, $\mathbf{F} = \partial \mathbf{x}(\mathbf{X}, t)/\partial \mathbf{X}$ is the deformation gradient, $\mathbf{x}(\mathbf{X}, t)$ gives the position of the material particle $\mathbf{X}$ at time t, $\mathbf{v} = \dot{\mathbf{x}}$ gives the velocity of the material particle $\mathbf{X}$, a superimposed dot indicates the material time derivative, $\mathbf{T}$ is the first

Communicated by S. N. Atluri, 13 September 1995

R. C. Batra
Department of Engineering Science and Mechanics, Virginia Polytechnic Institute and State University, Blacksburg, VA 24061, USA

Z. Peng
27124 Yorkshire Sq. #108, Dearborn Heights, MI 48127, USA

Correspondence to: R. C. Batra

This work was supported by the U.S. Army Research Office grant DAAH04-95-1-0042 and the NSF grant CMS-9411383 to the Virginia Polytechnic Institute and State University.

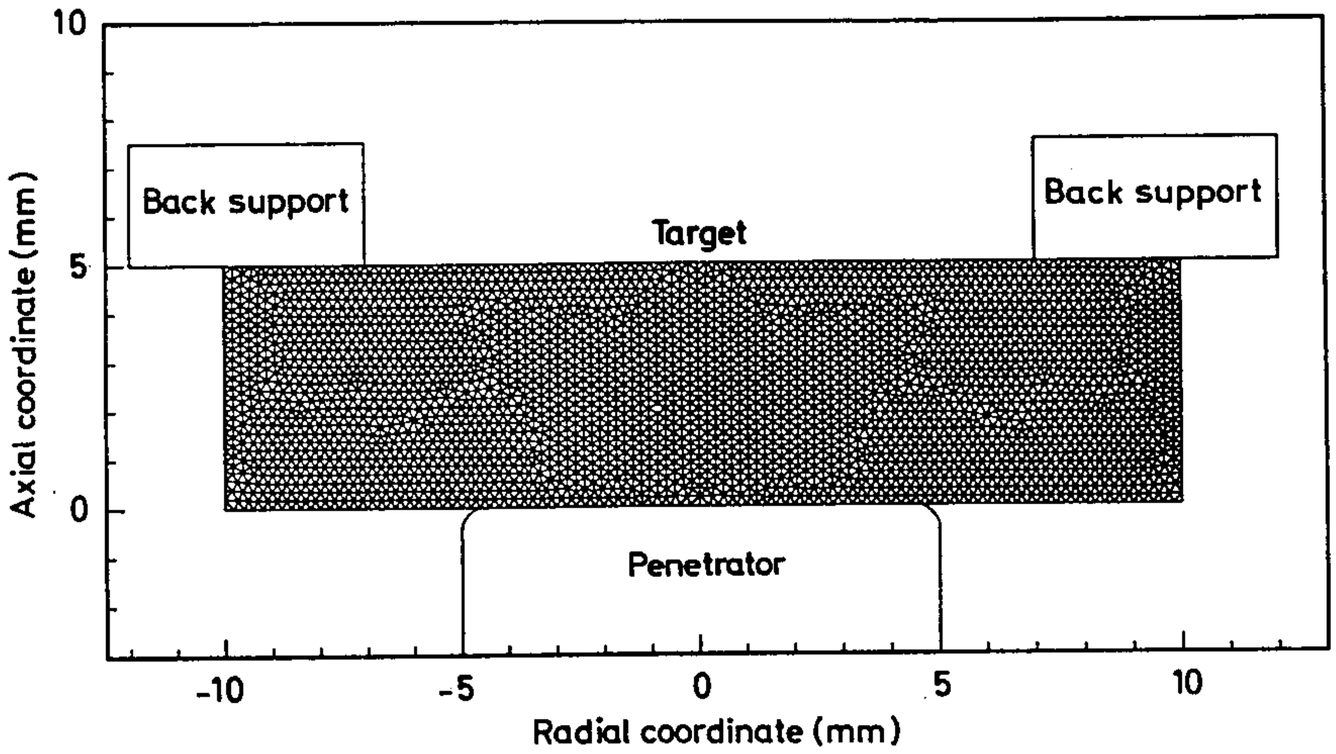

Fig. 1. A schematic sketch of the problem studied and initial discretization of the plate

Piola-Kirchhoff stress tensor, e is the specific internal energy, and Q the heat flux measured per unit reference area. The operator Div indicates the divergence operator with respect to coordinates in the reference configuration. Equations (1)–(3) are supplemented with the following constitutive relations.

$$\boldsymbol{\sigma} = -p(\rho)\mathbf{1} + 2\mu\bar{\mathbf{D}}, \quad p(\rho) = K(\rho/\rho_0 - 1) \tag{4}$$

$$2\mu = \frac{\sigma_0}{\sqrt{3}I}(1 + bI)^m(1 - v\theta)\left(1 + \frac{\psi}{\psi_0}\right)^n, \quad 2I^2 = \mathrm{tr}(\bar{\mathbf{D}}\bar{\mathbf{D}}^T), \tag{5}$$

$$\dot{\psi} = 4\mu I^2 \Big/ \left(1 + \frac{\psi}{\psi_0}\right)^n \sigma_0, \quad \bar{\mathbf{D}} = \mathbf{D} - \tfrac{1}{3}\mathrm{tr}(\mathbf{D})\mathbf{1}, \tag{6}$$

$$\mathbf{T} = J\boldsymbol{\sigma}(\mathbf{F}^{-1})^T, \quad \mathbf{Q} = J\mathbf{q}(\mathbf{F}^{-1})^T, \quad \mathbf{q} = -k\,\mathrm{grad}\,\theta, \tag{7}$$

$$\rho_0\dot{e} = \rho_0 c\dot{\theta} + p\dot{\rho}/\rho^2. \tag{8}$$

Here $\boldsymbol{\sigma}$ is the Cauchy stress tensor, K the bulk modulus, σ_0 the yield stress in a quasistatic simple tension or compression test, ψ an internal variable that describes the hardening of the material, k the thermal conductivity, c the specific heat and θ the rise in the temperature of a material particle. From $(4)_1$ and $(5)_1$ it follows that

$$(\tfrac{3}{2}tr(\mathbf{s}\mathbf{s}^T))^{1/2} = (1 + bI)^m(1 - v\theta)\left(1 + \frac{\psi}{\psi_0}\right)^n. \tag{9}$$

That is the material obeys the von Mises yield criterion and the yield stress depends upon the strain-rate, temperature and the work-hardening parameter ψ. The constitutive relation $(4)_1$ with μ given by $(5)_1$ was first proposed by Batra (1988). In it, σ_0, b, m, v, ψ_0 and n are material parameters; b and m describe the strain-rate hardening of the material, v its thermal softening and ψ_0 and n its work-hardening. Once $(1 - v\theta)$ equals zero, the material behaves like an ideal fluid. We note that in our work the volumetric deformations are considered to be elastic, the distortional or shear deformations are taken to be plastic, there is no unloading considered, and a material point is assumed to deform plastically at all times; however, the plastic strain-rate is extremely small for low values of the effective deviatoric stress. Also, there is no failure or fracture criterion considered.

The plate is taken to be initially stress free, at rest, at a uniform temperature and the initial work-hardening is set equal to zero. The rigid penetrator or the punch is assumed to be moving at a uniform speed V_0 and is taken to be huge so that its speed can be assumed to be uniform during the perforation process.

Here we assume that all of the plastic working is converted into heating or equivalently have taken the Taylor-Quinney parameter equal to 1. Batra and Adulla (1994) have shown that a lower value of the Taylor-Quinney parameter delays the initiation of a shear band but has no effect on the qualitative nature of results.

For the boundary conditions we take $\mathbf{v} = \mathbf{0}$ and $\mathbf{q}\cdot\mathbf{n} = 0$ at the plate particles abutting the rigid supports, and $(\mathbf{v}\cdot\mathbf{n})\mathbf{n} = V_0\mathbf{n}$, $\mathbf{q}\cdot\mathbf{n} = 0$ at the smooth target/penetrator interface where $\mathbf{n}$ is a unit normal at a point on the interface. Thus the plate is assumed to be glued to the rigid stationary back supports and there is no interpenetration of the plate material into the punch. Should a gap develop between the plate and punch surfaces, the plate particles there are assumed to be traction free and thermally insulated. Because of the rather very short time duration of the punching process, the assumption of no heat transfer from the target into either the supports or the penetrator is a reasonable one.

The above-stated problem is highly nonlinear and too difficult to solve analytically; therefore, we seek its approximate solution by the finite element method.

3 Computation and discussion of results

In order to compute numerical results, we assigned following values to various parameters for the steel.

$$\sigma_0 = 792\ \mathrm{MPa}, \quad K = 157\ \mathrm{GPa}, \quad b = 10000\ \mathrm{sec},$$

$$v = 0.66 \times 10^{-3}/^{\circ}\mathrm{C}, \quad m = 0.01, \quad n = 0.09, \quad k = 50\ \mathrm{W/m\,^{\circ}C},$$

$$\rho_0 = 7840\ \mathrm{Kg/m^3}, \quad \theta_0 = 25\ ^{\circ}\mathrm{C}, \quad \psi_0 = 0.017, \quad c = 477\ \mathrm{J/Kg\,^{\circ}C}$$

In the computer code used to analyse the problem, the lumped mass matrix obtained by the row-sum technique is used. The element load vectors are evaluated by using the three-point quadrature rule. The coupled nonlinear ordinary differential equations obtained by using the Galerkin approximation are integrated by the forward-difference method which for linear problems is explicit and only conditionally stable. Because only volumetric elastic deformations are considered, the bulk wave speed is used to compute the time step size. Also, this time step size is checked against the critical time step size for the heat equation and the smaller of the two values is selected. After every time increment, the coordinates of nodes are updated and elements are checked for excessive distortion. If any interior angle of an element becomes less than 15°, the mesh is refined and the values of solution variables at the newly created nodes are interpolated from those at the nodes of the previous mesh. The mesh refinement subroutine of Batra and Ko (1992) is employed with the modification that the generated mesh is suitably graded. We recall that the goal of refining the mesh is to make $\int_{\Omega_e} Id\Omega$ nearly the same for each element in the mesh. Since this may generate a poorly graded mesh, the generated elements are suitably modified to create a proper

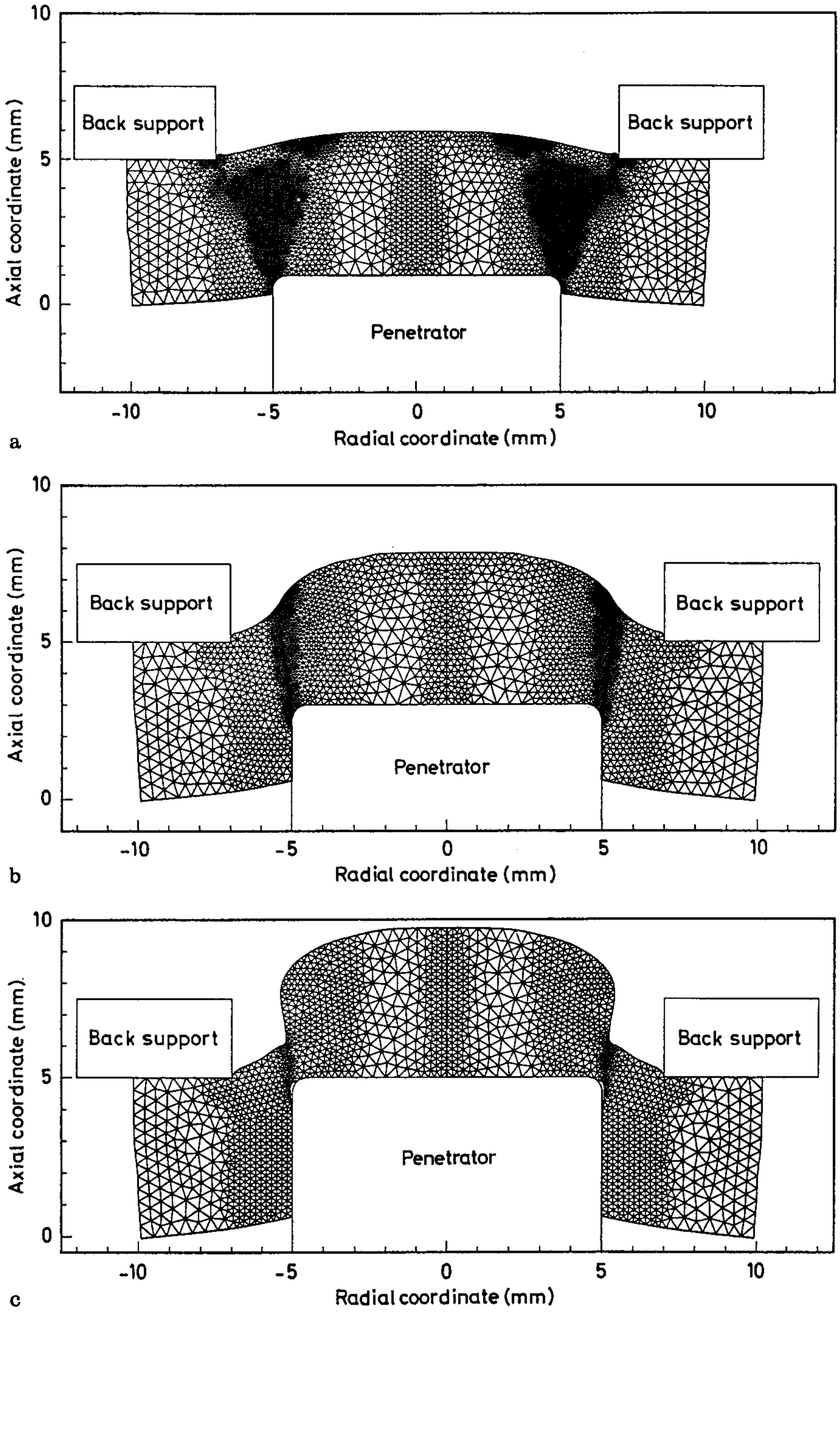

Fig. 2a–c. Deformed shapes of the plate and the refined meshes for subsequent computations when the penetration depth equals (a) 1 mm, (b) 3 mm, and (c) 5 mm; the penetrator speed is 50 m/s

grading of the mesh. The condition of impenetrability between the target and penetrator particles is satisfied by using the slideline algorithm of Hallquist et al. (1985); the rigid penetrator or punch surface is regarded as the master surface and the adjoining surface of the deformable plate as the slave surface, nodes on it and elements sharing at least one side with the penetrator/plate interface are called slave nodes and slave elements respectively. After each time increment, we find the normal acceleration of each slave node relative to the master surface. If this relative normal acceleration points away from the master surface, the node is released and is presumed not to be in contact with the master surface during the next time step. However, if the relative normal acceleration of a slave node is towards the master surface and its distance from the master surface is less than a preassigned small number, the slave node is taken to be on the master surface during the subsequent computations. We note that our method of accounting for the contact at the target/penetrator interface is a slight modification of that employed by Chen and Batra (1995).

Figures 2a, 2b and 2c depict the deformed shapes of the plate and the adaptively refined meshes used during subsequent computations when the penetration depth equals 1, 3 and 5 mm for an impact speed of 50 m/s. It is clear that significant bending deformations of the plate occur. We add that deformations of only one-half of the plate were analysed even though sketches drawn are for the full plate. Around the nose periphery, the target particles are separated from the penetrator surface; this separation is a function of the radius of the nose surface near its periphery. The plots of the velocity distribution within the deforming plate region indicate that at a penetration depth of 1 mm, the particles move both in the axial and radial directions but at a penetration depth of 5 mm and beyond, the target particles ahead of the punch move axially with the speed of the punch. As shown in Fig. 3, the axial velocity of particles decreases from that of the punch to essentially zero over the distance between the punch surface and the inner surface of the back rigid supports. Thus for a clearance of 2 mm and a punch speed of 50 m/s, the nominal strain-rate equals 25000/s and the primary mode of deformation is shearing. Once all of plate particles ahead of the punch surface move only axially, the plug has formed and is subsequently extruded from the plate. The temperature rise and deformed shapes of the plate at penetration depths of 2, 4 and 5 mm are shown in Figs. 4a, 4b and 4c respectively. These plots illustrate that only narrow regions of the plate adjacent to the vertical surface of the penetrator are heated up significantly. That these regions are deformed severely becomes clear from the contours of the work-hardening parameter ψ plotted in Fig. 5. We note that values of ψ are proportional to the effective plastic strain. A reasonable hypothesis is that fracture will occur along the surface of maximum effective plastic strain or equivalently that of maximum temperature. Thus the mantle of the plug ejected out of the plate will not have straight vertical surfaces. Results illustrated in Fig. 6 indicate that the shape of the plug depends noticeably upon the radius of the nose periphery; for a blunt nosed penetrator the mantle of the plug is essentially straight but has rather sharply inclined surface when the radius of the nose periphery is increased. Also the temperature rise for a penetration depth of 5 mm is maximum for the blunt-nosed penetrator.

Even though plate particles adjacent to the inner surface of the back support are also deformed severely, these do not seem to propagate into the plate. However, those of plate particles near the nose periphery of the punch propagate into the plate.

Batra and Zhang (1994) studied torsional deformations of a thin tube and called the speed of propagation of the contour of effective plastic strain of 2.0 as the speed of the shear band. We note that in general, an exception being the torsional deformations studied by Batra and Zhang, the computed speed is a function of the value of the effective plastic strain, e.g. see Zhu and Batra (1991). For the material model used herein, the internal variable ψ is a measure of the work-hardening and hence plastic strain at a material point. We have plotted in Fig. 7 plate regions wherein ψ exceeds 1.5 when the penetration depth equals 2.2 mm, 2.4 mm and 2.6 mm; from these the average speed of propagation of the contour of $\psi = 1.5$ is found to be 71.4 m/s. As was done by Chou et al. (1991), we define the distance of the tip of the contour of $\psi = 1.5$ from the penetrator nose surface as the shear band length, and plot it versus the penetration depth in Fig. 8a for three different values of the radius of the nose periphery. Thus an increase in the value of the edge radius delays the initiation of the shear band. Since the horizontal axis is proportional to the time elapsed from the instant the punch just touched the plate, the slope of these curves is proportional to the band speed. Thus the band speed increases with the penetration depth and is nearly independent of the edge radius. Recalling that the formation and ejection of the plug essentially involves shearing of this material from the rest of the plate material resting on the rigid supports, one will conjecture that the development of the shear band depends noticeably upon the distance between the penetrator and the inner surface of the support or the clearance between the penetrator and the supports. Results plotted in Fig. 8b support this and indicate that at least for the flat nosed penetrator the shear bands initiate sooner and propagate faster as the clearance is reduced. The

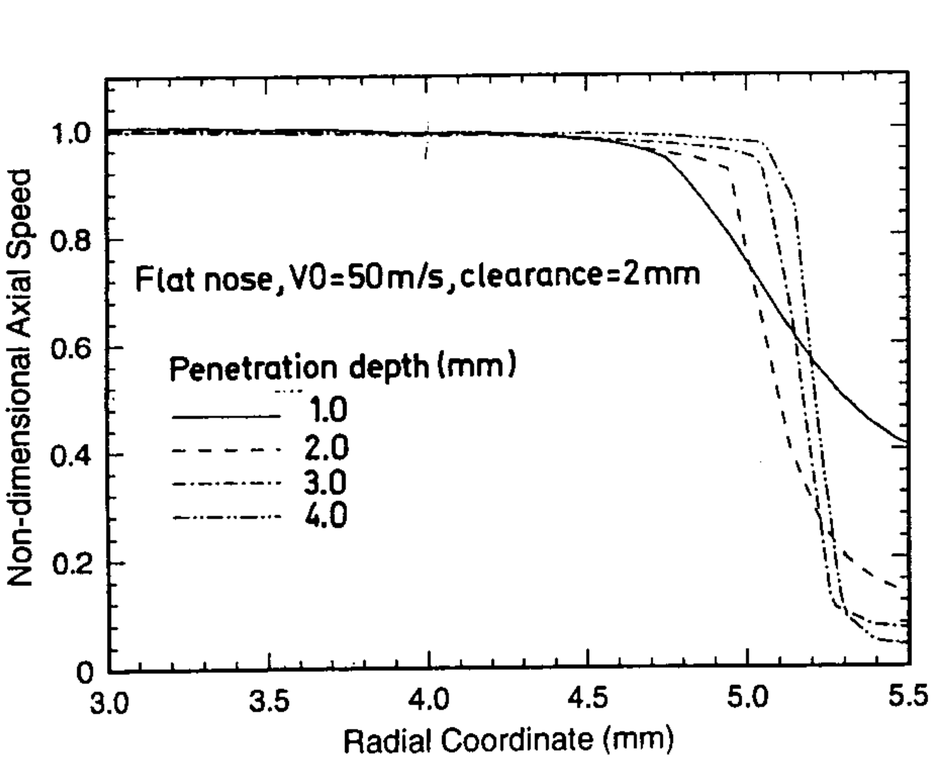

Fig. 3. Distribution of the non-dimensional axial velocity of plate particles that are 1 mm ahead of the punch nose surface when the penetration depth equals 1, 3 and 5 mm; the speed is non-dimensionalized with respect to that of the punch

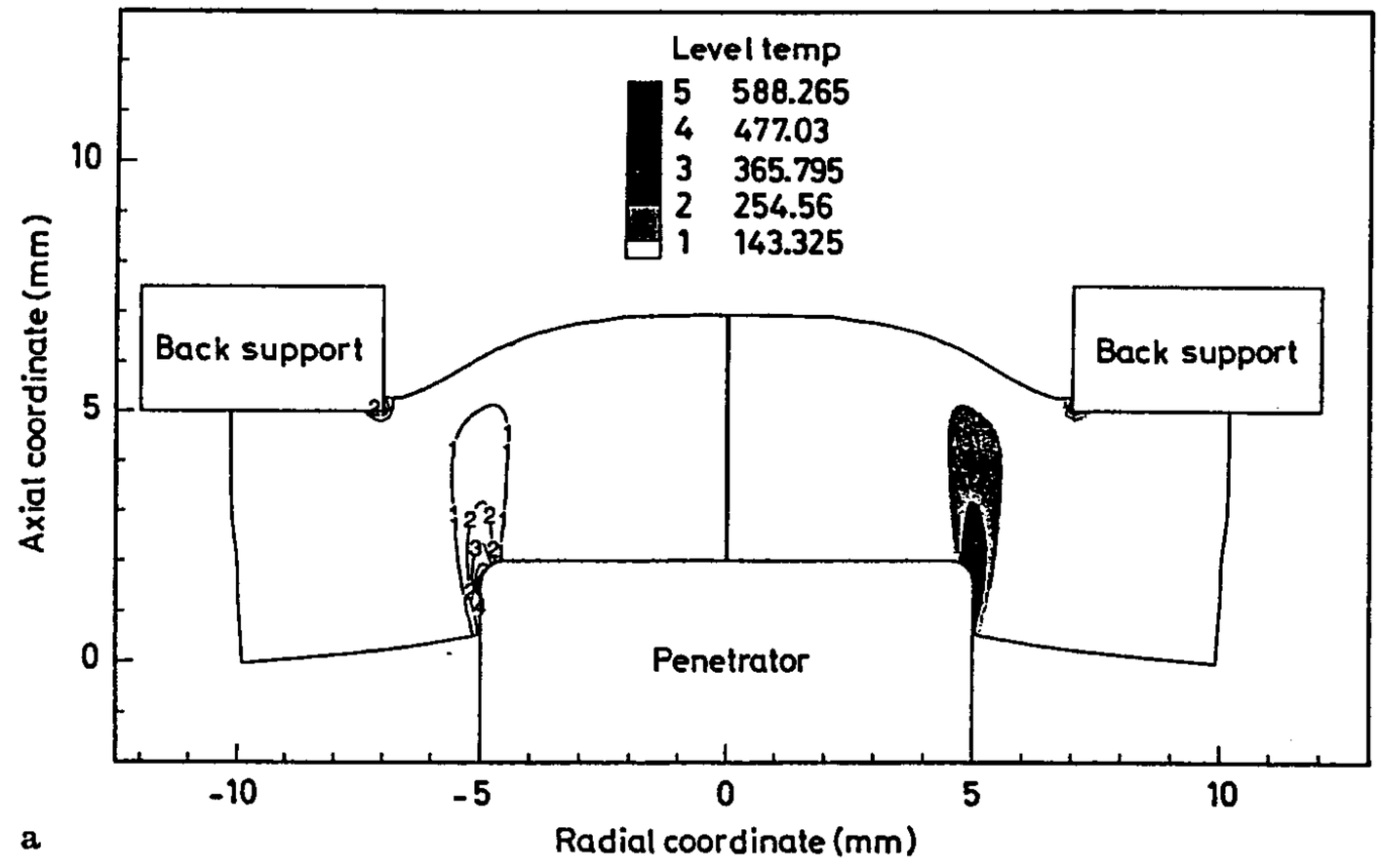

a

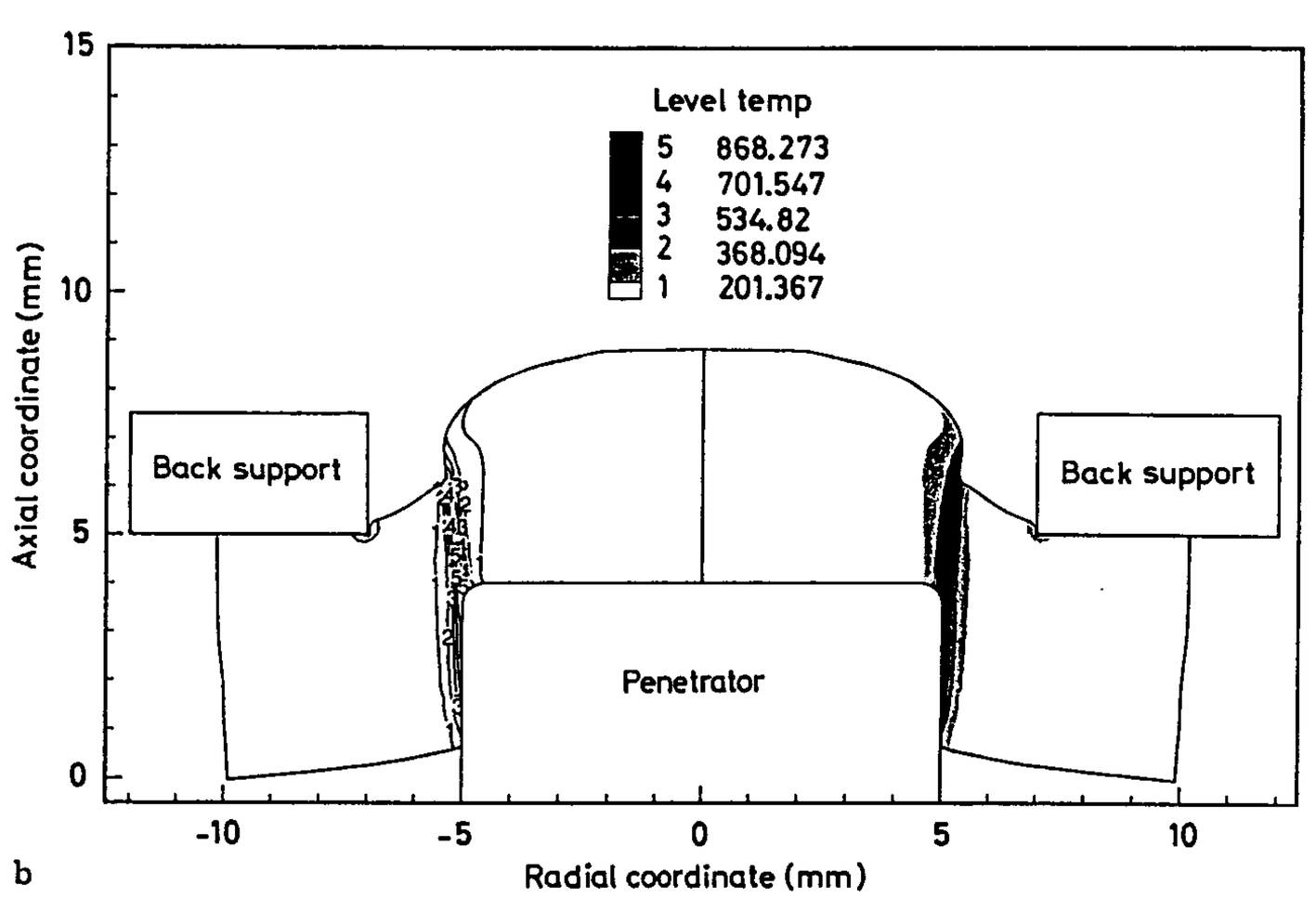

b

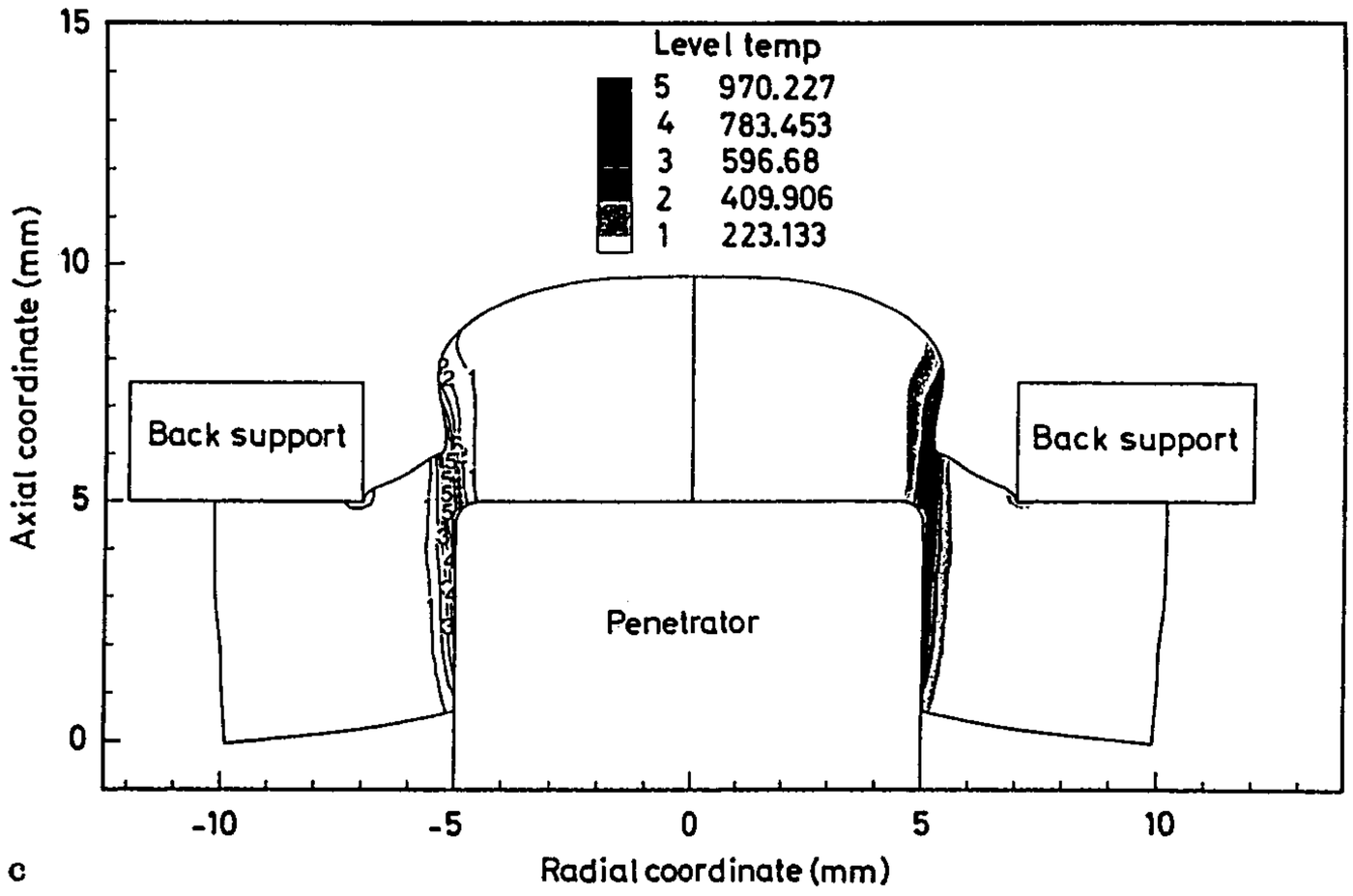

c

Fig. 4a–c. Distribution of the temperature rise in °C in the deformed plate when the penetration depth equals (a) 2 mm, (b) 4 mm, and (c) 5 mm

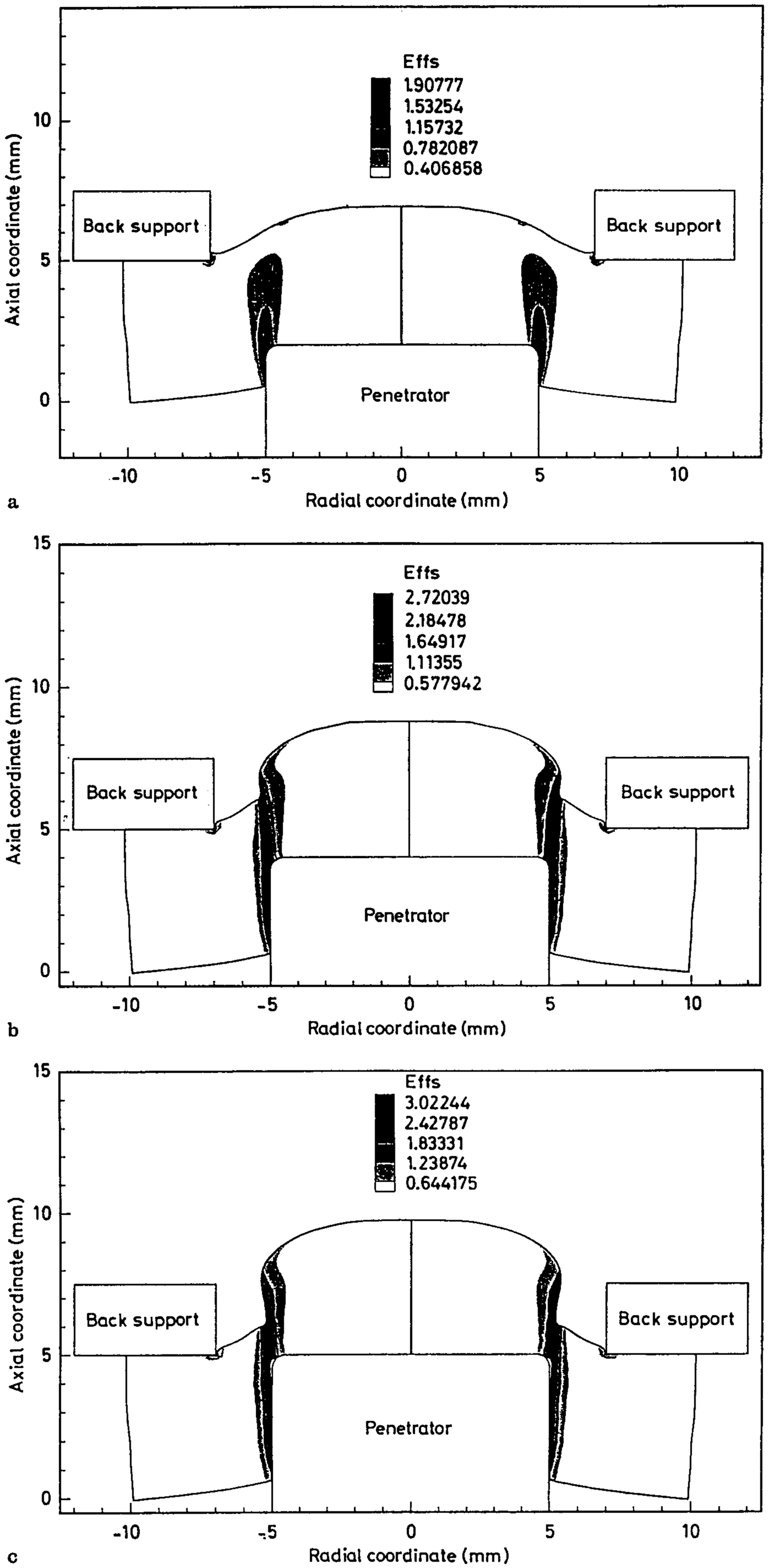

Fig. 5a–c. Contours of the work-hardening parameter ψ in the deformed plate when the penetration depth equals (a) 2 mm, (b) 4 mm, and (c) 5 mm

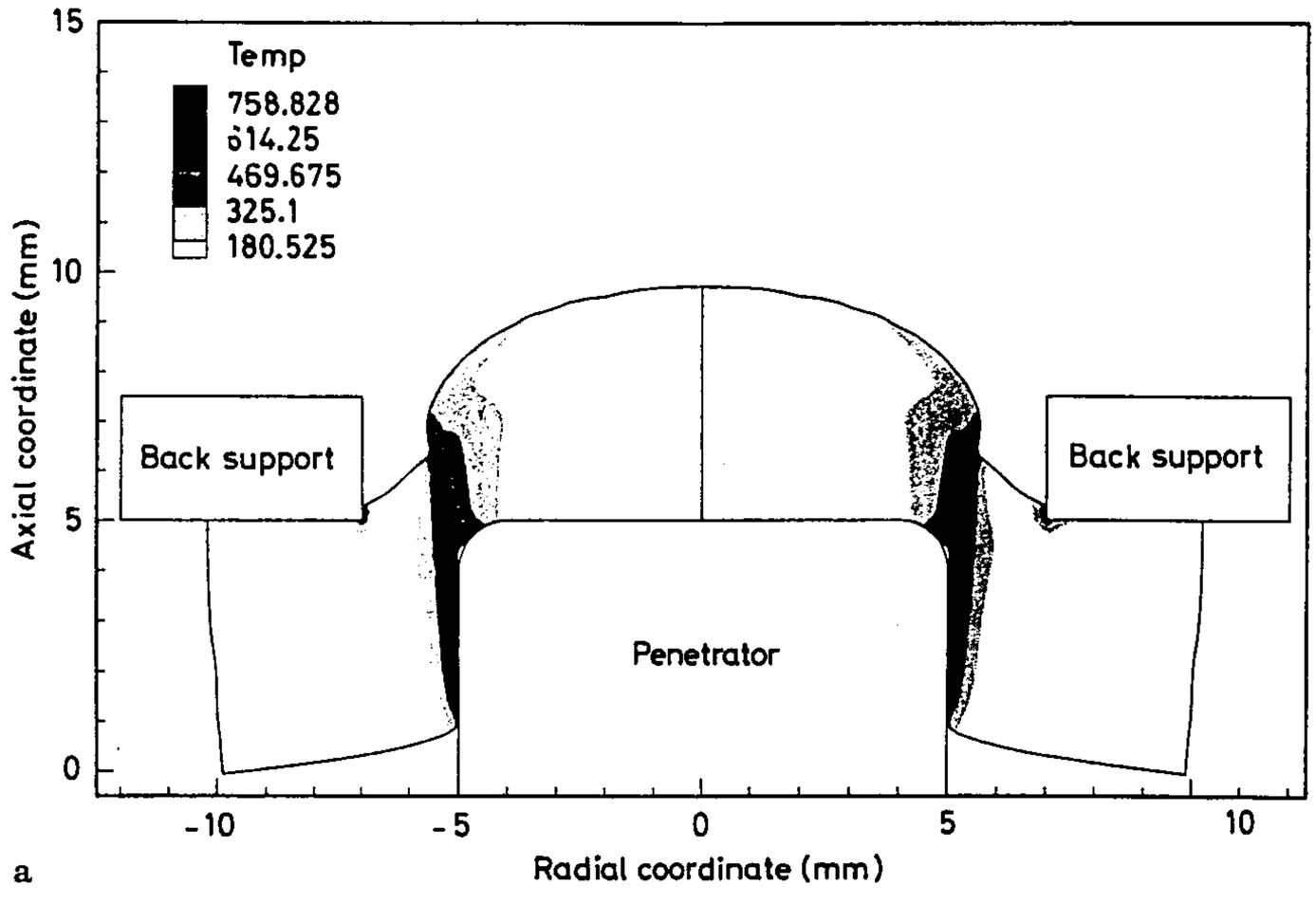

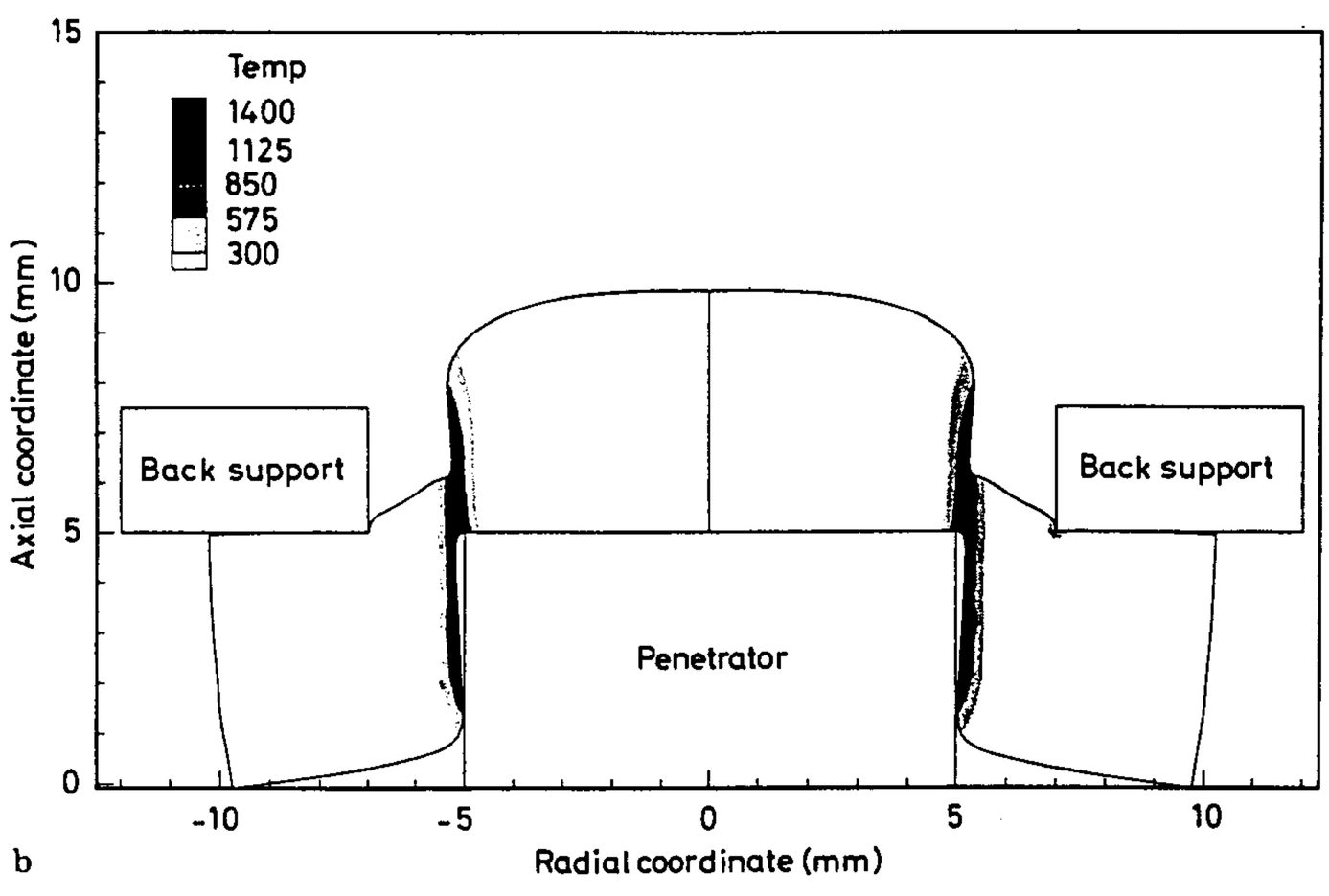

Fig. 6a, b. Contours of the temperature rise in °C in the deformed plate at a penetration depth of 5 mm (a) radius of the periphery of the nose of the punch equal to 1 mm, (b) flat-nose penetrator

smallest value, 500 μm, of the clearance considered herein is approximately 10 times the width of the shear band observed experimentally (e.g. see Moss (1981)) in steels. Figure 8c depicts the length of the shear band ahead of a flat-nosed penetrator as a function of the penetration depth for different values of the penetrator speed. The effect of punch speed manifests itself through an increase in the nominal strain-rate and hence affects the material response. From these curves it is hard to quantify the dependence of the shear band length ahead of the punch surface upon the penetration speed. These results could not be compared with the test observations of Chou et al. (1991) because of the lack of values for material parameters. However, they agree qualitatively with those plotted in their Fig. 2.

Even though we have used adaptively refined meshes to compute results, it is possible that these depend upon the smallest element size specified during the mesh refinement; this has not been explored. One way to get mesh independent results is to use a thermoviscoplasticity theory that incorporates a material characteristic length, e.g., see Wright and Batra (1985), Batra (1987) and Aifantis (1984).

4 Conclusions

We have studied the dynamic axisymmetric thermomechanical problem involving the perforation of a steel plate by a huge punch whose speed can be regarded as constant during the perforation process. The effects of inertia forces and heat conduction are considered. It is found that after the punch has traversed a certain distance into the plate, plate particles ahead of the punch face essentially move as a rigid

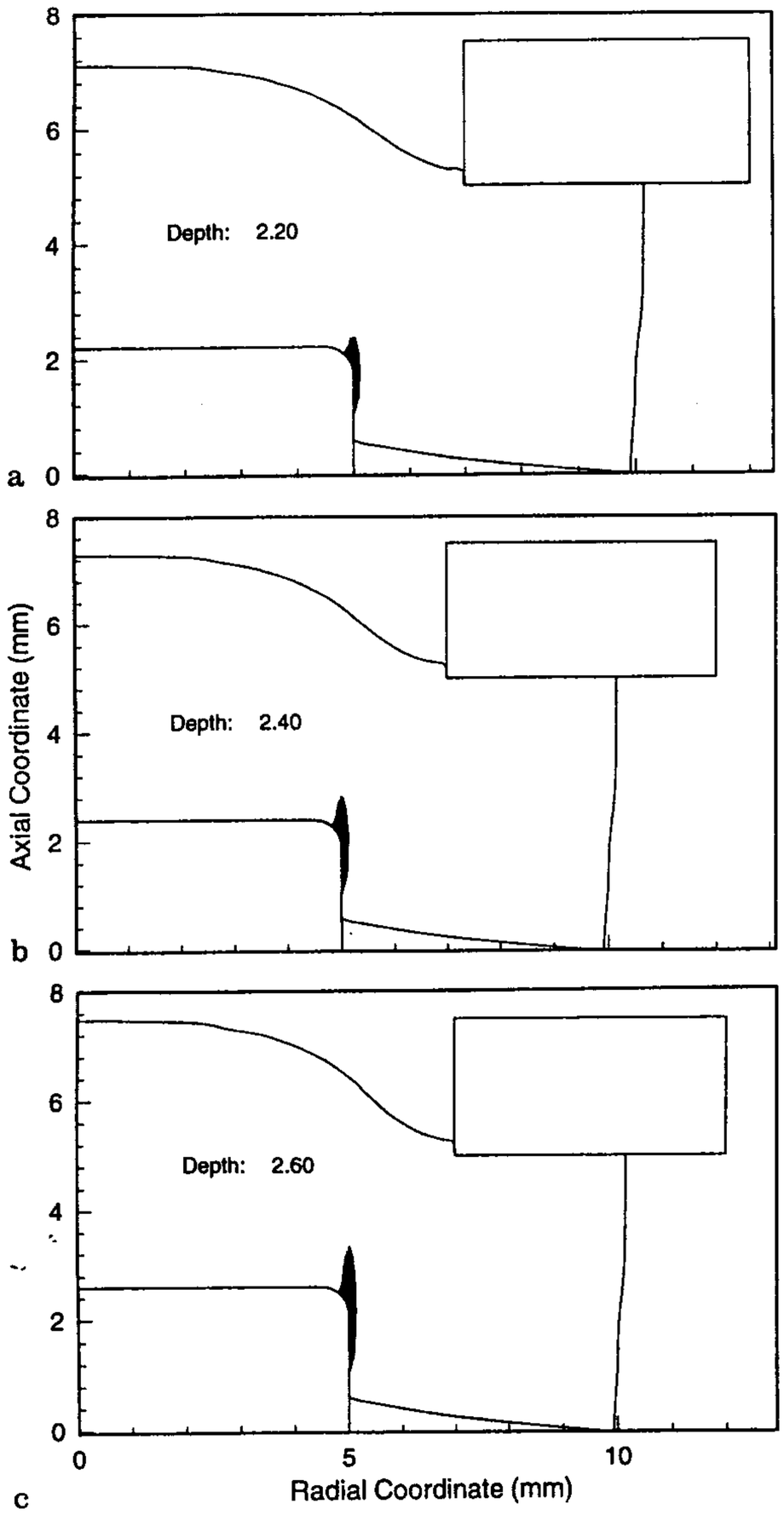

Fig. 7. Dark areas indicate regions wherein the value of the work-hardening parameter ψ equals at least 1.5

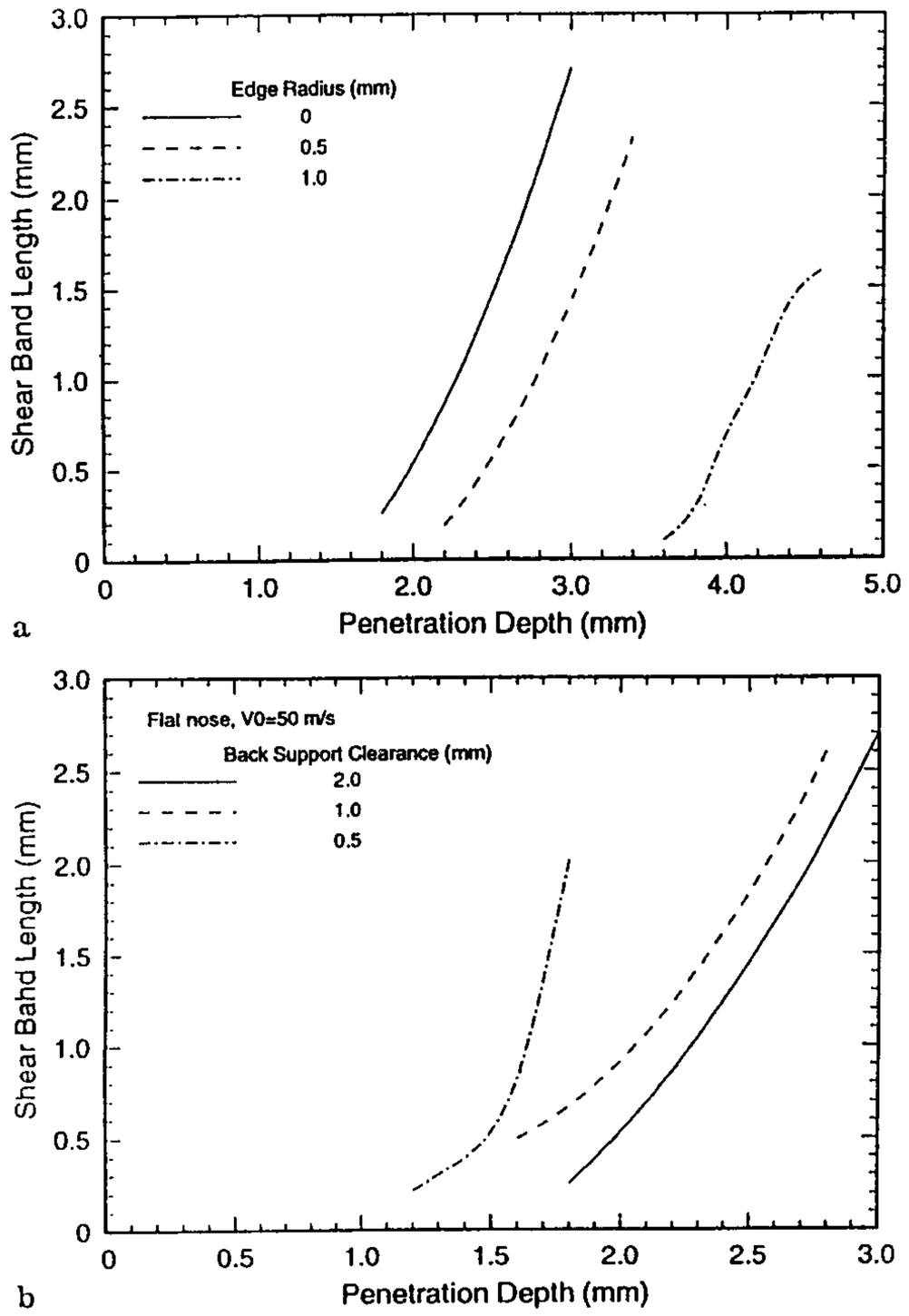

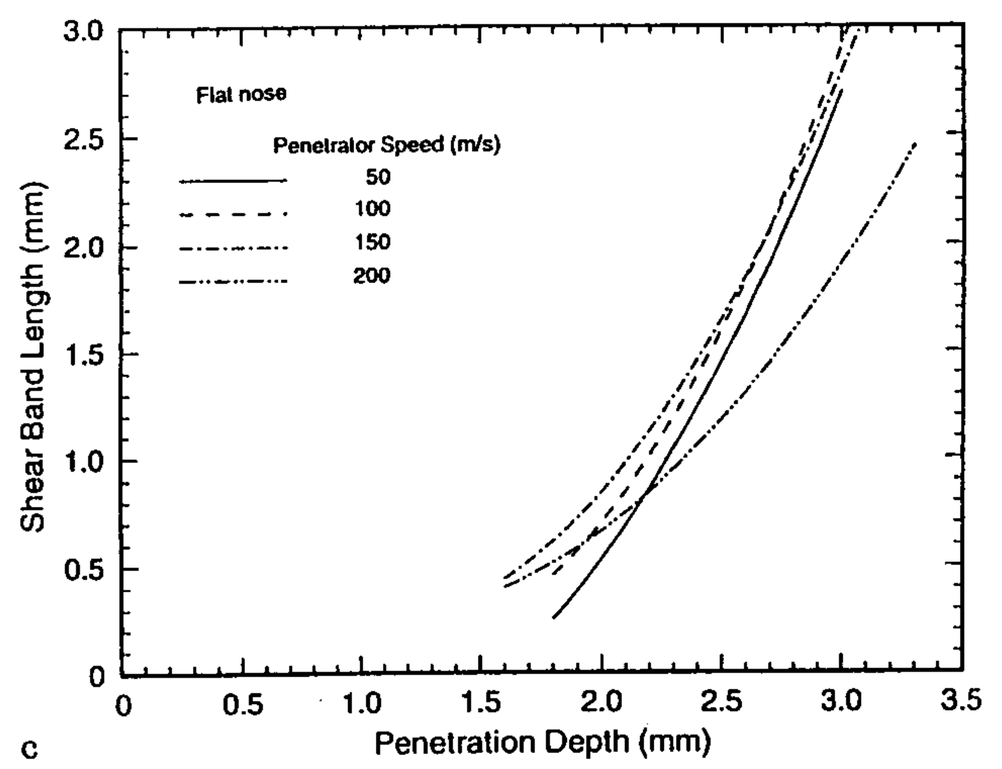

Fig. 8a–c. Effect of (a) the radius of the nose periphery, (b) the clearance between the punch and the supports, and (c) the punch speed, upon the length of the shear band ahead of the punch nose

body and this region is sheared from the remaining plate material resting on the flat rigid supports. Only a narrow cylindrical region of the plate adjacent to the mantle of the punch is severely deformed and the intensely deformed region propagates ahead of the punch surface into the plate. The clearance between the penetrator and the back supports as well as the radius of the periphery of the punch nose affect noticeably when a shear band initiates and the length of the shear band ahead of the punch surface. The average shear band speed, defined as the axial speed of the contour of the work-hardening parameter equal to 1.5, is computed to be 71 m/s; this speed depends upon, among other factors, the depth of penetration and the clearance between the penetrator and the supports. The maximum temperature rise also depends upon these factors and for the flat nosed penetrator equals 93% of the melting temperature of the steel.

References

Aifantis, E. C. 1984: On the microstructural origin of certain inelastic solids. J. Engr. Mat. Tech. 106: 326–330

Armstrong, R. W.; Batra, R. C.; Meyers, M. A.; Wright, T. W. 1994: Shear instabilities and viscoplasticity theories. Mechs. Mat. 17: 83–327

Bai, Y.; Dodd, V. 1992: Adiabatic shear localization, Occurrence, Theories, and Applications. New York: Pergamon Press

Batra, R. C. 1987: The initiation and growth of, and the interaction among adiabatic shear bands in simple and dipolar materials. Int. J. Plasticity 3: 75–89
Batra, R. C.; Adulla, C. 1994: Effect of prior quasistatic loading on the initiation and growth of dynamic adiabatic shear bands. In: (Noor, A. K. and Needleman, A. eds.) Computational Material Modeling. AD-Vol. 42, New York: ASME Press
Batra, R. C.; Zhang, X. T. 1994: On the propagation of a shear band in a steel tube. J. Eng'g Mat. and Tech. 116: 155–161
Batra, R. C.; Zbib, H. M. 1994: Material instabilities, theory and applications. New York: ASME Press
Batra, R. C.; Ko, K. I. 1992: An adaptive mesh refinement technique for the analysis of shear bands in plane strain compression of a thermoviscoplastic solid. Computational Mech. 10: 369–379

Batra, R. C. 1988: Steady state penetration of thermoviscoplastic targets. Computational Mech. 3: 1–12
Chen, X.; Batra, R. C. 1995: Deep penetration of thick thermoviscoplastic targets by long rigid rods. Computers and Structures. 54: 655–670
Chou, P. C.; Hashemi, J.; Chou, A.; Rogers, H. C. 1991: Experimental and finite element simulation of adiabatic shear bands in controlled penetration impact. Int. J. Impact Engng. 11: 305–321
Duffy, J. 1984: Temperature measurements during the formation of shear bands in a structural steel. In: (Dvorak, G. J. and Shields, R. T., eds.): Mechanics of material behavior. Amsterdam: Elsevier Science, B.V.
Hallquist, J. O.; Goudreau, G. L.; Benson, D. J. 1985: Sliding interfaces with contact–impact in large scale Lagrangian computations. Computer Methods in Appl. Mech. Engng. 51: 107–137
Kalthoff, J. F. 1987: Shadow optical analysis of dynamic shear fracture. Optical Engng. 27: 835–840
Marchand, A.; Duffy, J. 1988: An experimental study of the formation process of adiabatic shear bands in a structural steel. J. Mech. Phys. Solids. 36: 251–283
Mason, J. J.; Rosakis, A. J.; Ravichandran, G. 1994: Full field measurements of the dynamic deformation field around a growing adiabatic shear band at the tip of a dynamically loaded crack or notch. Mechs. Mat. 42: 1679–1697
Moss, G. L. 1981: Shear strain, strain rate and temperature changes in an adiabatic shear band. In: (Meyer, M. A. and Murr, L. E. eds.): Shock Waves and High Strain Rate Phenomenon in Metals. New York: Plenum Press
Tresca, H. 1978: On further application of flow of solids. Proc. Inst. Mech. Engr. 30: 301–345
Wright, T. W.; Batra, R. C. 1985: The initiation and growth of adiabatic shear bands. Int. J. Plasticity 1: 205–212
Zbib, H. M.; Shawki, T.; Batra, R. C. (eds.) 1992: Material instabilities. Appl. Mechs. Revs. 45: S3–S173
Zener, C.; Hollomon, J. H. 1944: Effect of strain-rate on plastic flow of steel. J. Appl. Phys. 14: 22–32
Zhu, Z. G.; Batra, R. C. 1991: Shear band development in a thermally softening viscoplastic body. Computers and Structures. 39: 459–472